Greenland Ice Sheet Melt from MODIS and Associated Atmospheric Variability

Sirpa Häkkinen, Dorothy Hall, Christopher Shuman, Denise Worthen and Nicolo DiGirolamo, Code 615, NASA GSFC

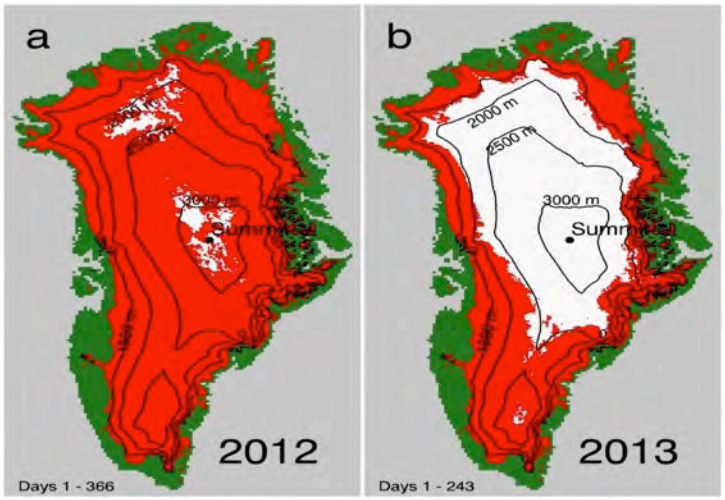

Figure 1: Maximum extent of melt on the Greenland Ice Sheet for 2012 (Panel a) and 2013 (Panel b) as determined from MODIS-derived melt maps. In clear-sky conditions, a maximum of ~95 % of the ice sheet surface (shaded red) experienced some melt in 2012 and only ~49 % of the ice sheet surface experienced some melt in 2013. White represents no melting (according to MODIS), and green represents non-ice covered land areas. Elevation contours are shown at 1500, 2000, 2500 and 3000 m.

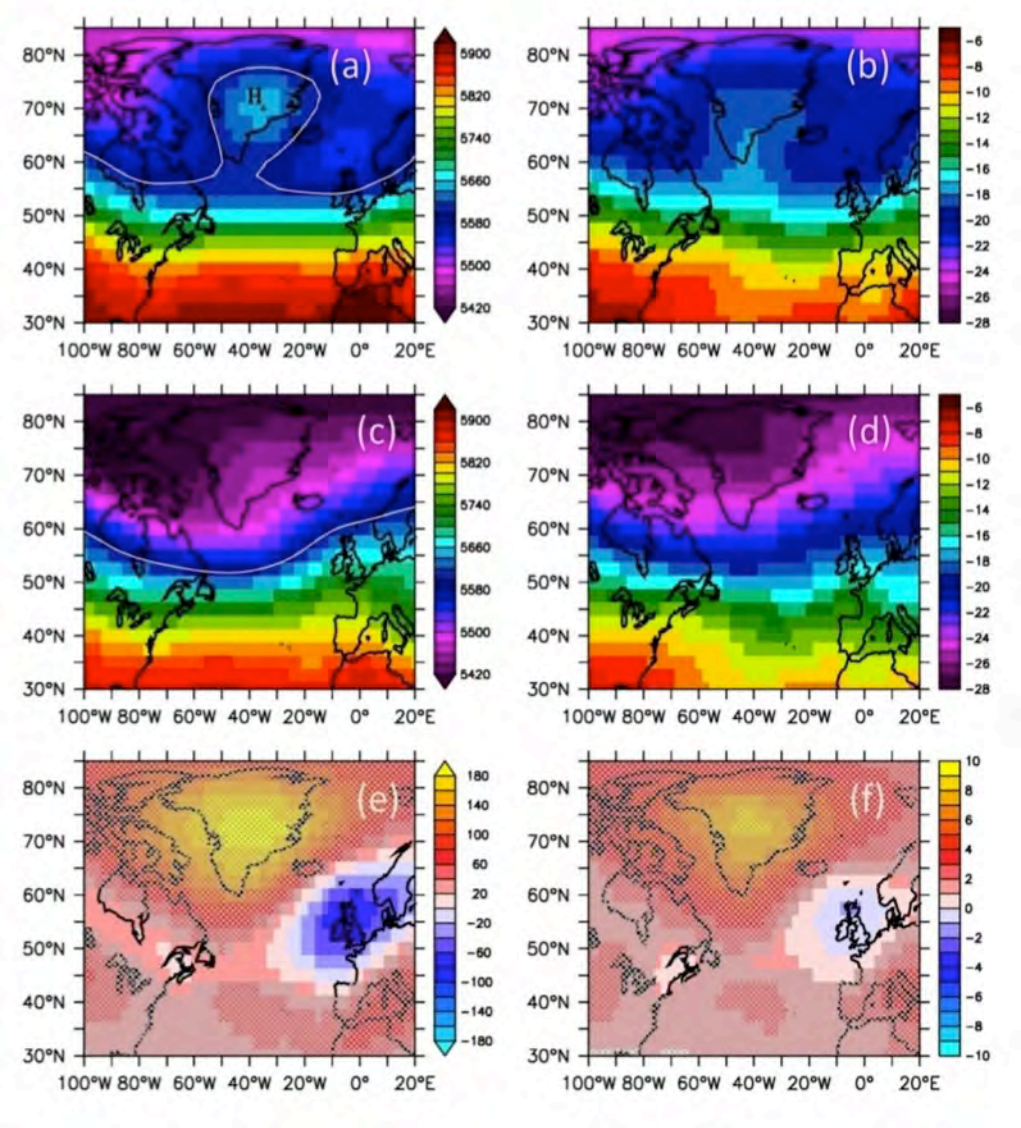

Figure 2: 2000 – 2013 composite of 500 hPa geopotential heights (meters) (left) and temperatures (°C) (right) when the MODIS melt anomaly (shown in Fig. 2) is stronger than +1 standard deviation (a, b), and less than -1 standard deviation (c, d). The difference is shown in (e,f) for (a)-(c), and (b)-(d) respectively. In a) and c) Z500=5600 m is drawn as a white contour; also in a) maximum Z500=5647 m is marked. The cross hatched values denote differences that are significant at the 99% level.

Name: Sirpa Hakkinen,NASA/GSFC, Code 615
E-mail: sirpa.hakkinen@nasa.gov
Phone: 301-614-5712

Abstract:

Comparison of summer 2012 and 2013 shows an extreme contrast in the maximum melt area from the MODIS-derived Greenland ice sheet (GIS) melt. Our study shows that daily variability of GIS melt and atmospheric conditions are closely linked and is attributed to atmospheric blocking over Greenland which brings warm subtropical air masses over the GIS. Blocking is a necessary condition for melt episodes but associated temperature anomalies are also important.

References:

Sirpa Häkkinen, Dorothy K. Hall, Christopher A. Shuman, Denise L. Worthen and Nicolo E. DiGirolamo: Greenland Ice Sheet Melt from MODIS and Associated Atmospheric Variability, *Geophys. Res. Lett.*, in press, 2014.

Dorothy K. Hall, Josefino C. Comiso, Nicolo E. DiGirolamo,Christopher A. Shuman, Jason E. Box, and Lora S. Koenig.: Variability in the surface temperature and melt extent of the Greenland ice sheet from MODIS, *Geophys. Res. Lett.*, 40, doi:10.1002/grl.50240, 2013.

Data Sources: MODIS ice-surface temperature (IST) and derived GIS melt fraction, 500hPa temperature and geopotential height from NCEP/NCAR Reanalysis.

Technical Description of Figures:

Figure 1: Maximum extent of melt on the GIS in 2012 and in 2013 according to MODIS (Hall et al., 2013). The actual extent of melt is somewhat greater than can be detected by MODIS since the MODIS IST maps are only obtained in clear-sky conditions. The IST is derived from a standard MODIS product and is accurate to ~1°C at surface temperatures near 0°C.

Figure 2: Atmospheric patterns: Omega-blocking pattern when there is a major GIS melt episode (a) and (b); zonal flow when cold conditions and minimal melt dominates (c) and (d); and the difference between these patterns for the 500 hPa height and temperature (e) and (f) (Häkkinen et al., in press).

Scientific significance:

Daily June-July melt fraction variations over the Greenland Ice Sheet (GIS) derived from MODIS (2000-2013) are associated with atmospheric blocking forming an omega-shape ridge over the GIS at 500 hPa height. Blocking activity with a range of time scales, from synoptic waves breaking poleward (< 5 days) to full-fledged blocks ($\geq$5 days), brings warm subtropical air masses over the GIS controlling daily surface temperatures and melt. Based on the years with the greatest melt (2002 and 2012) during the MODIS era, the area-average temperature anomaly of 2 standard deviations above the 14-year June-July mean results in a melt fraction of 40% or more. In contrast to summer 2012, summer 2013 had only a moderate amount of blocking days, and the associated area-average temperature anomalies were weak, barely reaching 1.5 standard deviations above the June-July (14-year) mean.

Relevance for future science and relationship to Decadal Survey:

We show that daily (area-average) air temperature at about 5 km height, about 2 km above the GIS summit, varies in-phase with MODIS IST in June and July, the months most likely to have intense melt events. MODIS IST provides a physical measurement of the surface conditions over the GIS consistent with the prevailing atmospheric conditions.

Spatial Scaling of Soil Moisture and Groundwater Variability

Matthew Rodell, Code 617, and Bailing Li, ESSIC and Code 617, NASA GSFC

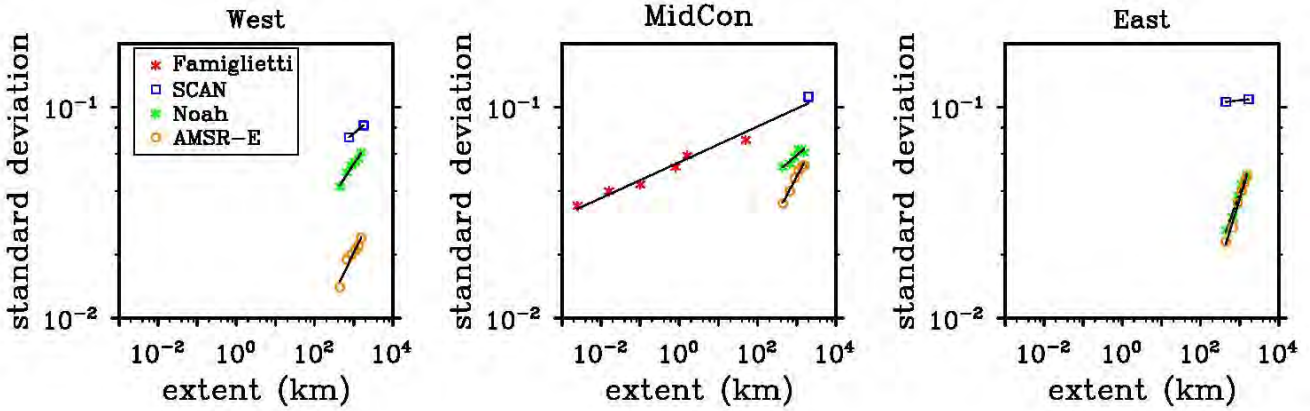

Figure 1: The spatial variability (as quantified by the standard deviation) of observed and modeled volumetric soil moisture (-) increases linearly with spatial extent when plotted on a log-log graph. Spatial extent was calculated as the square root of the area of each field site, observation network, or model region..

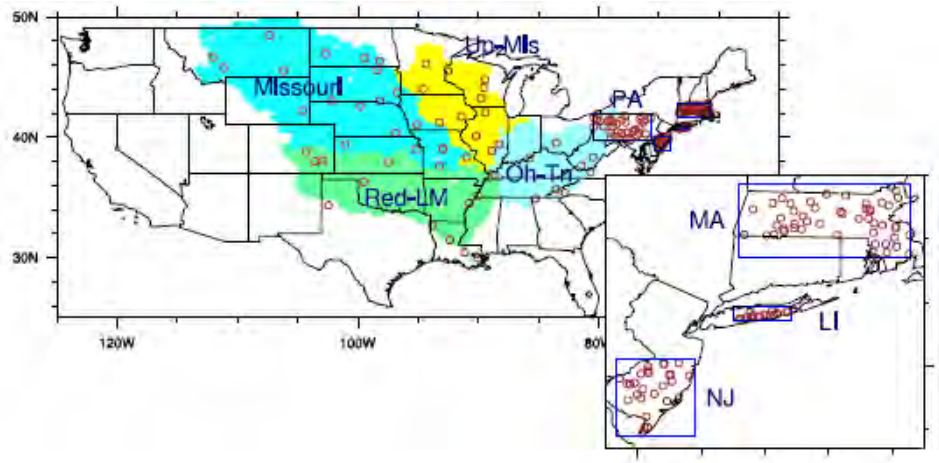

Figure 2: Locations of nine regions (shaded colors, including the whole Mississippi River basin and its four major sub-basins, and blue boxes) and groundwater monitoring wells (circles) that provided the data for Figure 3.

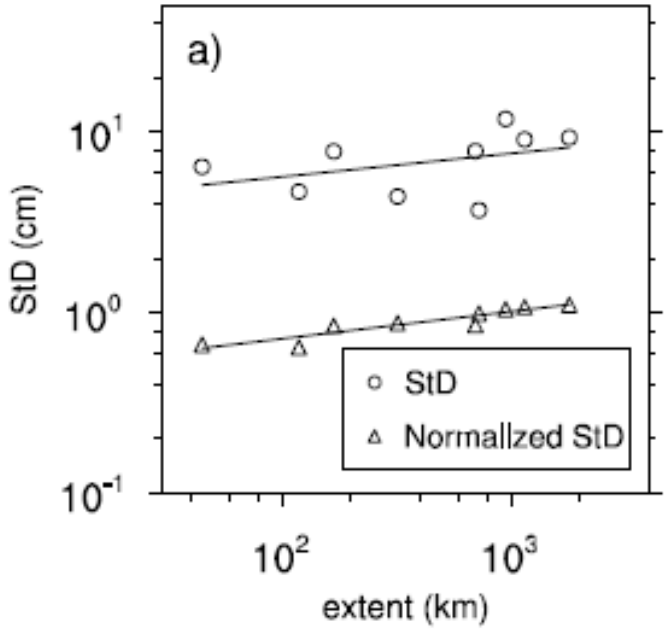

Figure 3: As with soil moisture, the spatial variability (standard deviation) of groundwater storage anomalies (deviations from the long term mean) increases linearly with spatial extent when plotted on a log-log graph. To remove the effect of differing climates, normalized standard deviation in a region was computed by dividing the spatial standard deviation by the average (over all wells in that region) of the long term temporal standard deviation. From Li et al. (2014).

Name: Matthew Rodell, NASA/GSFC, Code 617; and Bailing Li, ESSIC, NASA/GSFC, Code 617
E-mail: Matthew.Rodell@nasa.gov; Bailing.Li-1@nasa.gov
Phone: 301-286-9143

Abstract:
Previous studies have shown that the spatial variability of soil moisture increases linearly when plotted on a log-log graph against spatial extent, from scales of meters to tens of kilometers. We proved that this relationship extends to scales of hundreds of kilometers. Further, we demonstrated for the first time that the spatial variability of groundwater storage anomalies (deviations from the long term mean) exhibits the same behavior.

References:

Li, B., M. Rodell, and J.S. Famiglietti, Groundwater variability across scales in the central and eastern U.S., *Wat. Resour. Res.*, submitted, 2014.

Li, B. and M. Rodell, Spatial variability and its scale dependency of observed and modeled soil moisture over different climate regions, *Hydrol. Earth Syst. Sci.*, 17, 1177-1188, doi:10.5194/hess-17-1177-2013, 2013.

Data Sources: Soil moisture data were collected during the SGP97, SGP99, SMEX02, and SMEX03 field campaigns, measured by the SCAN network, and simulated by the NLDAS/Noah land surface model. Groundwater data were archived by the USGS and the Illinois State Water Survey.

Technical Description of Figures:

Figure 1: The spatial variability (as quantified by the standard deviation) of observed and modeled volumetric soil moisture (-) increases linearly with spatial extent when plotted on a log-log graph. Spatial extent was calculated as the square root of the area of each field site, observation network, or model region. Results are shown for the western, central, and eastern U.S. (left to right), using ground based measurements from a field campaign (Famiglietti) and an observation network (SCAN), numerically modeled soil moisture (Noah), and remotely sensed soil moisture (AMSR-E). From Li and Rodell (2013).

Figure 2: Locations of nine regions (shaded colors, including the whole Mississippi River basin and its four major sub-basins, and blue boxes) and groundwater monitoring wells (circles) that provided the data for Figure 3.

Figure 3: As with soil moisture, the spatial variability (standard deviation) of groundwater storage anomalies (deviations from the long term mean) increases linearly with spatial extent when plotted on a log-log graph. To remove the effect of differing climates, normalized standard deviation in a region was computed by dividing the spatial standard deviation by the average (over all wells in that region) of the long term temporal standard deviation.

Scientific significance:
The scaling relationships described here had previously been hypothesized but never demonstrated at regional to continental scales. While fascinating on their own, they are also valuable for interpreting and downscaling coarse resolution satellite observations of soil moisture and groundwater, for upscaling in situ observations, and for developing and evaluating hydrological models.

Relevance for future science and relationship to Decadal Survey:
Many remote sensing missions, including SMAP and GRACE FO, provide coarse resolution data which must be interpreted in such a way as to make them useful for fine scale practical applications. Further, the retrievals must be evaluated and calibrated using in situ observations, which requires an understanding of how soil moisture and groundwater variability scale spatially.

Oso Landslide in Snohomish County, Washington

Dalia Kirschbaum, Code 617, NASA GSFC

PHOTO BY TED S. WARREN /THE ASSOCIATED PRESS; GRAPHIC BY THE SEATTLE TIMES

Figure 1: Catastrophic landslide that took place on March 22, 2014 in Oso, Snohomish County, WA. The landslide appears to have been initiated by seasonal rainfall, among other factors, and shows a rotational slide at top with large mobilized mudflow features downslope.

Figure 2: Image from Landsat 8 pan-sharpened natural colour 15 m resolution data taken Sunday morning, March 23rd, 2014. Photo courtesy of Jesse Allan (Sigma Space Corp/NASA)

Figure 3: Cumulative rainfall (mm) for the regional rainy season (Oct-Mar) taken from 2000-2014. The red line indicates the 2014 rainy season and blue lines show previous years. According to TMPA RT data, this was the wettest season on record since 2004 and the 3rd wettest since the start of the TRMM record with a rapid increase in cumulative rainfall starting in February.

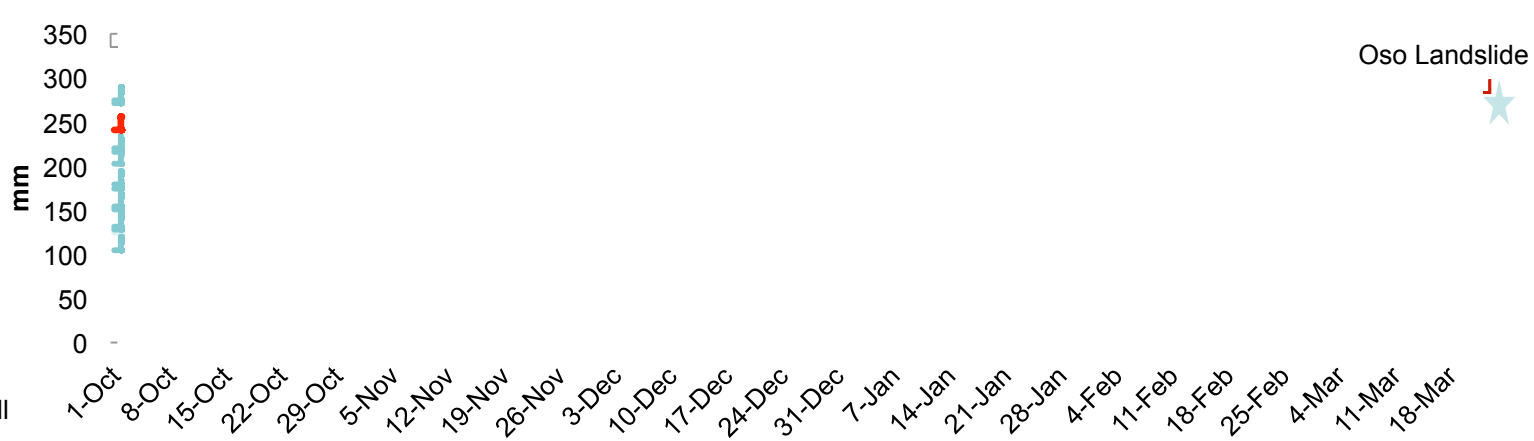

Landslide Hazard Assessment in Snohomish County, Washington

Dalia Kirschbaum, Code 617, NASA GSFC

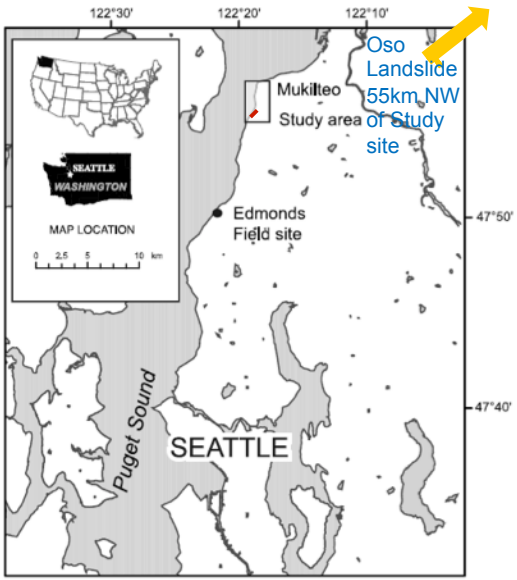

Figure 4: Observed landslides on the Mukilteo Speedway March 13, 2011. Potential failure zone (red) on Google Maps image: Imagery © 2014 Google, Map data © 2014 Google. Right figure from Baum et al. 2010.

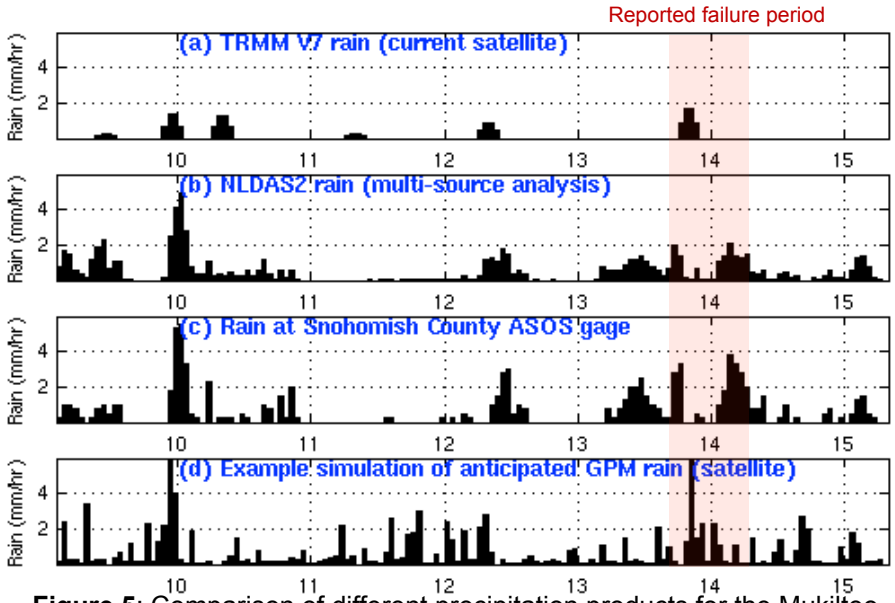

Figure 5: Comparison of different precipitation products for the Mukilteo Speedway event in March 2013 comparing TRMM, NLDAS2, gauge, and simulated GPM product.

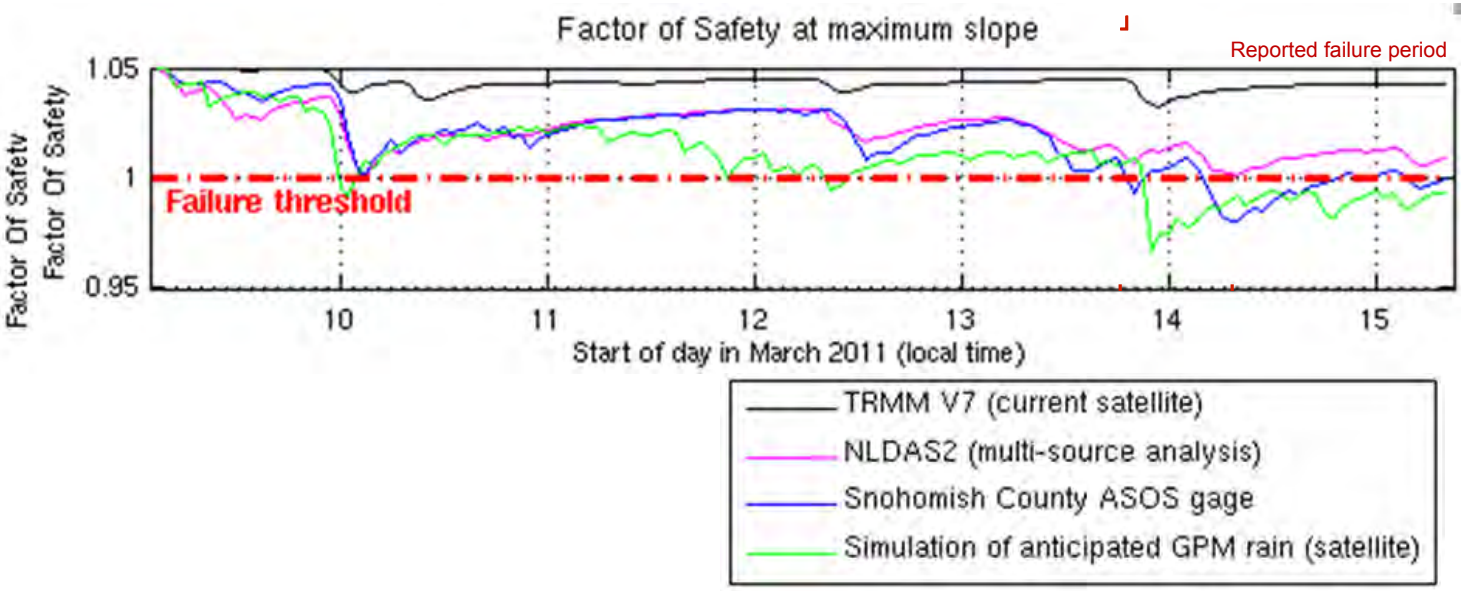

Figure 6: Evaluation of slope failure calculations for March 2011 event using a USGS slope-stability model (TRIGRS), testing several precipitation sources. A Factor of Safety below 1 indicates a potential landslide. Preliminary results indicate that while TRMM data could not resolve the landslide, gauge, NLDAS can model the landslide failure. Simulated GPM data is also shown to potentially improve upon TRMM to better resolve landslide-triggering rainfall in this area.

Name: Dalia Kirschbaum, NASA/GSFC, Code 617
E-mail: dalia.b.kirschbaum@nasa.gov
Phone: 301-614-5810

Abstract: This work investigates landslide events in Snohomish County, Washington, a place known for frequent and catastrophic slope failures. The first highlight slide provides an aerial photograph of the Oso Landslide that took place in the morning on March 22nd. This landslide occurred in the area previous landslides and was likely initiated as a result of above average rainfall in the area of the slide throughout the past rainy season. A Landsat 8 image provides a satellite view of the landslide area, allowing for a broader perspective of the morphology and area impacted. A retrospective analysis of TRMM Multi-satellite Precipitation Analysis (TMPA) data indicates that the 2013-14 rainy season was the wettest on record for TRMM since 2004 and the 3rd wettest season overall. The unique aspect of this rainfall is that the majority of the rainfall at this location occurs later in the season (February-March) relative to previous seasons, indicating there may have been a rapid increase in subsurface soil moisture and pore pressures that may have ultimately led to the catastrophic failure. Other evaluations of rainfall have suggested that the previous 30 days of rainfall were over 6 inches above average for the 30 day totals. The landslide model at Goddard was not able to resolve this event due to the limited rainfall amounts occurring in the days leading up to the event. Future work is underway to better account for antecedent rainfall and soil moisture, which can trigger catastrophic landslides such as the one at Oso.

The second slide highlights recent work conducted for an area of Snohomish County 55 km SW of the Oso landslide location. This work uses a slope-stability model called TRIGRS to evaluate the potential conditions for a landslide event, represented when the Factor of Safety dips below 1. Several different rainfall inputs were tested for an event reported along the Mukilteo Speedway from March 13, 2011 including rain gauge, modeled (NLDAS2), and TMPA data to evaluate the sensitivity of the TRIGRS model to various rainfall inputs. GPM data is not yet available to the public, so we used a model to simulate GPM data based on anticipated improvements in the GPM-IMERG algorithm as well as improved resolution of light rain and mixed phase precipitation (ice, rain, snow) over this complex region. Results indicate that TRMM does not adequately resolve the peak intensities or volume of rain needed to trigger a landslide, whereas gauge and NLDAS data does resolve a failure during the reported landslide period. Sample simulated GPM data indicates that we may expect improved performance with GPM, which will help to better resolve landslide-triggering rainfall in this region. Several other shallow landslides are being tested in the proximate area.

References:

Baum, R. L., Godt, J. W., & Savage, W. Z. (2010). Estimating the timing and location of shallow rainfall induced landslides using a model for transient, unsaturated infiltration. *Journal of Geophysical Research*, *115*(F03013). doi:10.1029/2009JF001321

Huffman, G. J., Adler, R. F., Bolvin, D. T., & Nelkin, E. J. (2010). The TRMM Multi-satellite Precipitation Analysis (TMPA). In F. Hossain & M. Gebremichael (Eds.), *Satellite Rainfall Applications for Surface Hydrology* (pp. 3–22). Springer Verlag.

Kirschbaum, D. B., Adler, R., Hong, Y., Hill, S., & Lerner-Lam, A. (2010). A global landslide catalog for hazard applications: method, results, and limitations. *Natural Hazards*, *52*(3), 561–575. doi:10.1007/s11069-009-9401-4

Yatheendradas, S., D. Kirschbaum, R. Baum, J. Godt (2013). Evaluating a slope-stability model for shallow rain-induced landslides using gage and satellite data. *Proceedings of World Landslide Forum*, Beijing China

Yatheendradas, S., D. Kirschbaum, R. Baum, J. Godt, V. Maggioni, Y. Tian (in preparation): "Using satellite rain input for physically-based slope stability models in landslide early warning: a Seattle case study"

Data Sources: Global Landslide Catalog, TRMM 3B42 V7, North America Land Data Assimilation (NLDAS2) precipitation data, Landsat 8, Google Earth, Photo taken from Seattle Times

Scientific Significance: Landslide modeling systems are significantly limited at the local scale by the availability of adequate in situ information (soil, geology) as well as triggering variables such as rainfall. This work introduces the recent Oso landslide and preliminary satellite imagery of this location. TMPA data was able to provide a 15+ year retrospective analysis of the rainfall conditions of the event indicating above average seasonal rainfall for this region. This region, however, is outside the orbital path of the TRMM satellite, which orbits from 35 degrees N-S. GPM, which orbits from 65 degrees N-S will cover this area and provide improved capabilities to estimate historical rainfall as well as provide key inputs landslide models where rain gauge or other ground based sources are not available. Preliminary results of the modeling activities for southwest Snohomish County indicate the potential improvements that GPM data may have in better resolving landslide events in these highly susceptible regions.

Relevance for future science and relationship to Decadal Survey: Precipitation information from TRMM and the Global Precipitation Measurement (GPM) mission (www.nasa.gov/gpm) already help and will expand the capabilities to evaluate landslide triggering scenarios both in real-time and retrospective cases. Modeled and satellite-based estimates of soil moisture information, such as from the SMAP mission, may also provide important clues to antecedent soil moisture status, allowing us to discern whether a previous rainfall event may play a role in future landslide activity.

Global Leaf Area Index Product Validation Good Practices

Editors: Richard Fernandes (CCRS), Stephen Plummer (ESA), Joanne Nightingale (NPL),
CEOS/WGCV/LPV Chairs: Gabriela Schaepman-Strub (U Zurich) and **Miguel O. Román (NASA/GSFC)**

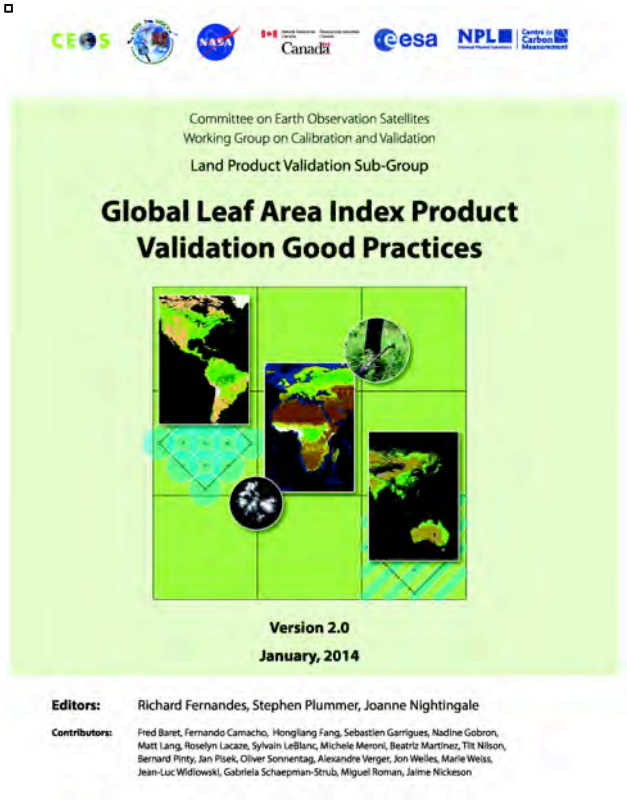

Figure 1: Global Leaf Area Index (LAI) Good Practices document developed by the Land Product Validation (LPV) sub-group of the CEOS Working Group on Calibration and Validation (WGCV): http://lpvs.gsfc.nasa.gov/documents.html

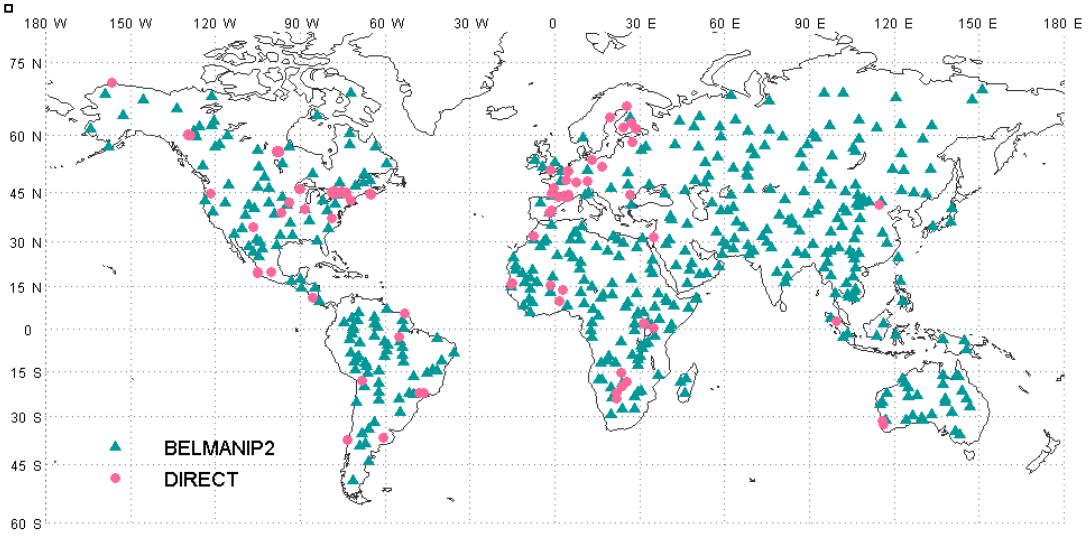

Figure 2: Location of reference LAI sites available for direct validation and inter-comparison studies.

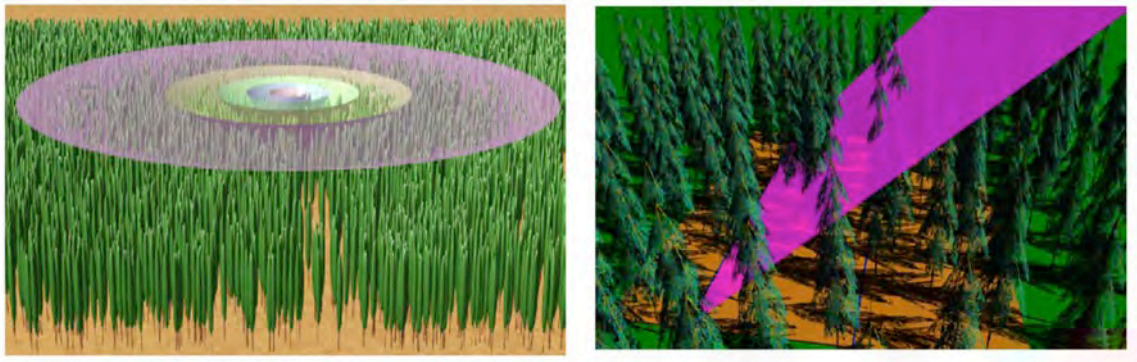

Figure 3: Depiction of spatial footprint of a LAI-2000 instrument as a function of zenithal view ring (left) and the TRAC instrument (right) for a given solar illumination condition.

Name: Miguel O. Román, NASA/GSFC
E-mail: Miguel.O.Roman@nasa.gov
Phone: 301-614-5498

Abstract: Benchmarking and comparison of satellite-derived Leaf Area Index (LAI) products is essential to resolve differences between products and to ensure their accuracy and reliability. When validation procedures are mature enough, they warrant development of internationally accepted good practices for validation. A recent best-practices document prepared by the CEOS Working Group on Calibration and Validation (co-chaired by Miguel Román - Code 619) provides those involved in producing and validating satellite based LAI products with a forum for documenting accepted best practices in an open and transparent manner that is scientifically defensible. This Global LAI product validation best practice protocol document (V2.0) has undergone scientific review by remote sensing experts from across the world. All comments and suggestions have been considered to formulate this consensus document and responses to reviewer concerns are logged alongside the protocol on the LPV webpage. A list of recommendations arising from findings in this document will be provided on the LPV webpage (http://lpvs.gsfc.nasa.gov/). It is expected the best practice protocol document and recommendations will undergo subsequent regular iterations based on community feedback and scientific advancement.

References: Fernandes, R.A., Plummer, S., Nightingale, J. eds. (2014), Global Leaf Area Index Product Validation Good Practices, version 2.0, Committee of Earth Observing Systems Working Group on Calibration and Validation: http://lpvs.gsfc.nasa.gov/documents.html .

Data Sources: This is a joint effort composed of multiple in-situ, airborne, and satellite datasets from different agencies; including the Canada Centre for Remote Sensing, the European Space Agency, NASA/GSFC's Terrestrial Information Systems Laboratory , and the UK National Physical Laboratory.

Technical Description of Images:

(Figure 1) The Global Climate Observing System (GCOS) has specified the need to systematically produce and validate global leaf area index (LAI) products. This document provides recommendations on best practices for the validation of global LAI products.

(Figure 2) Location of reference LAI sites available for direct validation and BELMANIP2 sites designated for product inter-comparison based on the OLIVE Validation Platform. (http://calvalportal.ceos.org/web/olive/site-description)

(Figure 3) Validation of satellite LAI products relies on aspects specific to satellite measurements. An Elementary Sampling Unit (ESU) is a contiguous spatial region over which the expected value of LAI can be estimated through in situ measurement. The ESU corresponds to the finest spatial scale of LAI estimates used for reference LAI maps. The ESU size is at least as large as one measurement footprint of the in situ instrument and typically includes a number of instrument measurements. The maximum ESU size is determined by the level of within ESU LAI variability that can be tolerated by the validation protocol and the effort available to conduct measurements. The size of each ESU within a reference region also varies with surface condition, instrument field of view, illumination conditions (when transmission based measurements are used) and spatial sampling design. This figure indicates the sensitivity of the measurement field of view to canopy and illumination conditions for two common instruments (LAI-2000 and TRAC).

Scientific significance: In response to GCOS Action Item T30, the goal of this document is to identify good practices for validating global satellite LAI products. The document specifically addresses accuracy assessment against reference LAI measurements. The latter is made traceable to in situ measurements of known accuracy and the assessment augmented with metrics of precision derived from ensembles of products themselves.

Relevance for future science and relationship to Decadal Survey: This document provides those involved in producing and validating satellite based leaf area index (LAI) products, including future Land Science missions (e.g., NASA HyspIRI and ESA SENTINEL) with a forum for documenting accepted best practices in an open and transparent manner that is scientifically defensible. This Global LAI product validation best practice protocol document (V2.0) has undergone scientific review by remote sensing experts from across the world. All comments and suggestions have been considered to formulate this consensus document and responses to reviewer concerns are logged alongside the protocol on the LPV webpage. A list of recommendations arising from findings in this document will be provided on the LPV webpage (http://lpvs.gsfc.nasa.gov/).